

Approximate third integrals for axisymmetric potentials using local Stäckel fits

De Bruyne V., Leeuwin F. and Dejonghe H.

Astronomical Observatory, Gent University, Krijgslaan 281 S9, B-9000 Gent, Belgium

13 June 2021

ABSTRACT

We use a set of Stäckel potentials to obtain a local approximation for an effective third integral in axisymmetric systems. We present a study on the feasibility and effectiveness of this approach. We have applied it to three trial potentials of various flattenings, corresponding to nearly ellipsoidal, disk and boxy density isophotes. In all three cases, a good fit to the potential requires only a small set of Stäckel potentials, and the associated Stäckel third integral provides a very satisfactory, yet analytically simple, approximation to the trial potentials effective third integral.

Key words: galaxies: structure, galaxies: elliptical and lenticular, galaxies: kinematics and dynamics, methods: analytical, methods: numerical

1 INTRODUCTION

It is well-known that axisymmetric potentials do not in general allow a global and isolating third integral in addition to the energy and the component of the angular momentum along the symmetry axis. However, for many axisymmetric potentials, numerical experience shows that the majority of orbits are constrained by an effective third integral over a large number of orbital periods. As appears from modeling observed galaxies, a third integral is often required to describe their dynamical structure (*e.g.* Binney et al. 1990; Dejonghe et al. 1996). Hence, it seems unescapable that distribution functions depending *a priori* on three integrals should be available for general models of elliptical galaxies.

In a stellar dynamical context, the problem of approximating the effective third integral is logically connected to the philosophy behind the construction method of dynamical models for galaxies: obviously, numerical models can do with numerical, or even implicit third integrals, while analytical models need analytical approximations.

Amongst the numerical modelling methods, those based on Schwarzschild’s approach (Schwarzschild 1979) are undoubtedly the most direct ones. In a given potential, a library of orbits is computed, while the time-averaged properties of the orbits are stored. The orbit library is supposed to sample integral space. A reproduction of the observables is sought by combination of orbits, populated with a non-negative number of stars (*e.g.* Rix et al. 1997; van der Marel et al. 1998). This powerful and very general technique allows to construct general three-integral models, without any explicit reference to the third integral, since in principle orbits can be labelled using any phase-space point on them. Spectral

analysis offers the possibility to simplify the expression for the orbits and to reduce storage requirements for the orbits (Binney & Spergel 1982; Papaphilippou & Laskar, 1996 & 1998; Valluri & Merritt 1998; Carpintero & Aguilar 1998).

However, for this type of modeling methods, the computational cost is relatively high. Moreover, smoothing is necessary because the singular boundaries of the orbital densities produce a fairly awkward sum of numerical functions, and the distribution function is a numerical function out of which the physical content may not be very easily extracted. The implicit reference to a third integral, which makes Schwarzschild methods so flexible, is at the same time a handicap for extracting information about the role played by this integral.

Analytical techniques would be more explicit. But no expression for a global third integral is known in general axisymmetric potentials – except for Stäckel potentials (*cf.* de Zeeuw 1985; Dejonghe & de Zeeuw 1988). Therefore analytical approximations have been built using perturbation methods. Systems deviating moderately from spherical symmetry have been considered, and an approximate integral derived, which reduces to the total angular momentum in the spherical limit (see Petrou 1983). Gerhard & Saha (1991) report on the use of three different perturbation techniques applied to a model that is initially spherical. (1) Methods based on the KAM theory, which have a validity that is often restricted to very small perturbations. In practice they find indeed that, whatever their order, these methods fail to track changes in the phase-space topology that occur when spherical symmetry is broken by a significant amount. (2) The averaging method (see *e.g.* Verhulst 1979; de Zeeuw & Merritt 1983) in their example also fails to track the box-orbits ($L_z = 0$)

that emerge in a flattened system, and it gives at first-order only a rough approximation to the third integral. (3) Finally, a resonant method using Lie transforms does yield a good approximation to the third integral. It tracks the new orbital families emerging around resonances, and may in principle be carried on to high order. The analytical expressions are however rather intricate, specially for orders higher than 1.

The last technique has been used at first-order by Dehnen & Gerhard (1993) to construct three integral oblate models for the perturbed isochrone sphere. An application to the boxy E3-E4 galaxy NGC 1600 has recently been presented by Matthias & Gerhard (1999).

However, one may need to model a galaxy with a potential that is far from any known integrable potential, so that global perturbation techniques become ineffective. An alternative approach is then to derive a so-called ‘partial integral’. The idea is that a third integral that can be easily determined for certain groups of orbits is probably also a good approximation for similar orbits. de Zeeuw, Evans & Schwarzschild (1996) and Evans, Häfner & de Zeeuw (1997) derived such a partial integral for thin and near-thin tube orbits in scale-free potentials.

Yet another well known approach is the use of separable potentials. One is led to this idea because motion around the origin can be expanded in a Taylor series and, since the lowest-order non-zero terms are quadratic, can be described as perturbed harmonic motion. Moreover, van de Hulst (1962) has shown that motion around the origin can be seen as (unperturbed) motion in a Stäckel potential. Basically, one then uses a much enlarged set of reference integrable potentials instead of merely quadratic ones. The Stäckel potential is found by fitting term to term the Taylor series for the original potential (up to quartic terms) to the expansion for the Stäckel potential. Local fits of similar nature have been performed by de Zeeuw & Lynden-Bell (1985) and Kent & de Zeeuw (1991), who applied it to the solar neighbourhood, by expanding the effective potential in the vicinity of circular orbits.

However, such a local fitting does not work for all orbits. For instance, it may fail for orbits with large radial extent. In many cases, though, an orbit can still be approximated by motion in a Stäckel potential provided that the potential is chosen to be a good average approximation to the true potential in the region covered by that particular orbit (see Kent & de Zeeuw 1991). A report on the calculation of such a good average and global approximation to the Galactic potential, together with some indications for the numerical implementation, can be found in Dejonghe & de Zeeuw (1988) and Batsleer & Dejonghe (1994).

In this paper, we want to improve the generality of the application of this family of potentials. We propose to obtain a set of local approximations to the potential using Stäckel potentials, each of which is an average approximation to the original potential in some region. Rather than expanding around an equilibrium point, which would make the extent of the region where the approximation holds difficult to handle, we partition integral space and fit the potential in the corresponding regions of configuration space. We use the QP method (Dejonghe 1989) to adjust each local Stäckel potential. Section 2 describes this. Once the set of local Stäckel potentials is obtained, we proceed by checking the quality of the orbits representation, and of the approximation for an

effective third integral, where it exists. Obviously, we do not expect to describe the eventual stochastic motion this way. Moreover, we may not be able to reproduce all minor orbital families. These questions are also addressed in section 2. In section 3 the actual fitting procedure is explained. Its performance is illustrated with three trial potentials, which correspond to mass densities with *resp.* nearly ellipsoidal, boxy and disky isophotes. These trial potentials are presented in section 4. The results can be found in section 5. Section 6 gives a discussion on the application of the method and the conclusions are given in section 7.

2 THE DESIGN OF THE SET OF STÄCKEL POTENTIALS

2.1 The principle

Orbits with a given set of integrals (E, J) , with E the (positive) binding energy and J the component of the angular momentum along the rotation axis, fill a certain volume \mathcal{S} in space (a meridional section of it is shown in figure 1b). The intersection of this volume with a meridional plane is called the zero velocity curve (ZVC). One proves easily that orbits with a set of integrals (E', J) , with $E' > E$ fill a volume that is completely embedded in the volume filled by orbits with the set of integrals (E, J) . Similarly, orbits with E and J' larger than J , have a ZVC that lies inside the ZVC defined by (E, J) . This means that all orbits in the shaded rectangle labeled \mathcal{R} in integral space (see figure 1a) will remain interior to the shaded region indicated as \mathcal{S} in Fig 1b. Any distribution function defined over \mathcal{R} in integral space can therefore be associated with a potential that needs only be defined in \mathcal{S} . Hence, a subdivision of the (E, J) -plane into a number of rectangles \mathcal{R} , is equivalent to subdividing space into a number of bounded domains \mathcal{S} . For each of these domains, a Stäckel potential can be determined that is locally a good approximation to the original potential. If in the end, the whole (E, J) -plane is covered by a set of rectangles $\mathcal{R}_{(E, J)}$, also space will be covered by a set of domains $\mathcal{S}_{(E, J)}$, and the original potential will be completely fit by a set of locally fitted Stäckel potentials.

2.2 Practically

In practice, the specification of a set of rectangles \mathcal{R} in integral space is equivalent to the specification of a grid, each gridpoint of which being the ‘upper left corner’ of \mathcal{R} . A grid in E can be constructed by dividing the system into equal mass shells and computing the circular orbit energy for each shell radius. For every value of E , we consider an equidistant grid in J , with 7 values in the interval $]0, J_{\max}(E)[$, the upper bound corresponding to the circular orbit with that energy (see also figure 2).

In Stäckel potentials, orbits are determined by three integrals of motion (E, J, I_3) . Following van der Marel et al. (1998), the different third integrals are parametrized with angles ω_i , that correspond to the angle between the horizontal axis and the radius to the most external of the two points where the orbit intersects the ZVC (see figure 2). The point of the ZVC where $I_3 = I_{3\max}$ is found. This is the point where the thin tube orbit touches the ZVC.

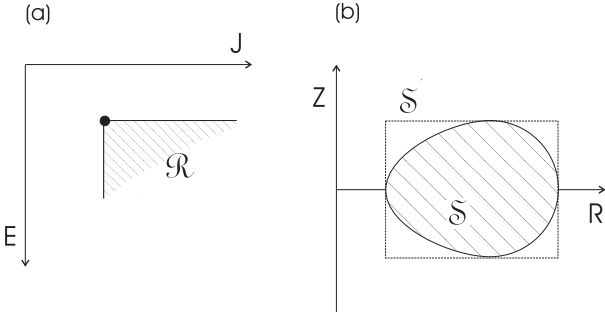


Figure 1. Panel (a): A rectangle \mathcal{R} in integral space, of which the ‘upper left corner’ corresponds to a gridpoint (E, J) . Panel (b): All orbits with $E' \geq E$ and $J' \geq J$ will remain interior to the region \mathcal{S} . In practice, the local Stäckel potential is determined in the rectangle \mathcal{S}' .

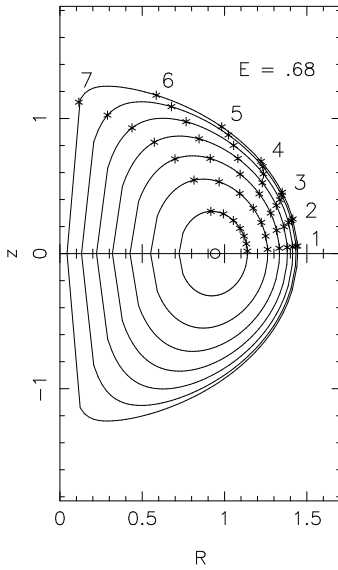


Figure 2. For one value of E in the grid : zero velocity curves corresponding to 7 different values for J and points used to determine 7 values for I_3 .

The coordinates (R, z) of that point determine the angle $\omega_{\max} = \pi - \text{Arctan}(z/(R - R_c(E)))$. The ω_i are chosen linearly between 0 and ω_{\max} , from which the values for $I_3(\omega_i)$ are derived.

As for the fit itself, it suffices to perform the Stäckel fit to the potential associated with a rectangle $\mathcal{R}_{(E,J)}$ only in the region interior to the velocity curve $\mathcal{S}_{(E,J)}$. In practice, we fit within the smallest rectangle $\mathcal{S}'_{(E,J)}$ which encompasses $\mathcal{S}_{(E,J)}$.

The construction of a set of potentials that covers the complete system potential is a multi-step process. It is most efficient to start with a global fit to the potential, i.e. fitting a Stäckel potential in the most extended domain \mathcal{S}' , determined, e.g., by the data. This domain defines the smallest value for E . The following steps improve the fit to the potential by performing a number of local fits in smaller domains.

The choice of domains where a fit will be performed is in principle arbitrary, and depends only on how well

the Stäckel potential has to approximate the system potential (within the limitations of what a regular potential can achieve).

2.3 When is a fit considered to be a good fit?

The fit is checked by comparing orbits in both potentials. Orbits start from the ZVC defined by (E, J) , at the point determined by the value of I_3 . The integration of orbits uses a fourth-order Runge-Kutta scheme with variable time-steps, proportional to the smallest of the radial and azimuthal periods, estimated respectively as $T_R \sim R/V_R$ and $T_\Omega \sim 2\pi R^2/J$. This ensures conservation of energy over $100 T_\Omega$ with a precision better than 10^{-6} .

One can consider various criteria for the comparison:

- *Surfaces of section:* The Stäckel potential should generate orbits that are very similar to those in the original potential. A first inspection can be done by comparing surfaces of section (SoS’s) in both potentials. What we mainly expect to find this way is:

- the proportion of non-regular orbits. If there is no additional integral of motion besides E and J , the orbits should fill uniformly the area bounded by the zero velocity curve on their SoS (Richstone 1982). If there is a third effective integral (effective meaning over the time the orbits are integrated), orbits are regular, and appear as curves on the SoS. Experience has taught that in axisymmetric models, stochastic orbits exist only for very small values of J . In models with a core, as considered here, these orbits are due to the large excursions in R and z for small J , which allow resonances between the two degrees of freedom (Merritt 1999).

- the minor families of orbits which may be present around some resonances in the original potential, that our Stäckel potential does not generate. We call them unrecovered minor families. The thin tube orbit at fixed (E, J) determines the main orbital family. This family encircles the origin on the (z, v_z) SoS, or a point $(R_{th}, 0)$ on the (R, v_R) SoS, where $R_{th}(E, J)$ is the point where the thin-tube orbit of given (E, J) intersects the equatorial plane. Minor orbital families may be generated by other resonances than the ones for small J , and will show up on a SoS as ‘islands’ surrounding other points.

- *Orbital densities:*

Since the Stäckel potential is aimed to be used for modeling, which is essentially assembling orbits to fit a given density, a good reproduction of the orbital densities is important.

These orbital densities $\nu(R, z; E, J, I_3)$ are functions of (R, z) for each given orbit, defined for any set (E, J, I_3) . The orbital densities for both potentials can be compared by measuring the fraction of the mass that is located in the same place in both potentials. If the total mass of every orbit is normalised to 1, and the cells surface is constant over the grid, the mass fraction correctly located (MC) can be calculated as

$$MC = 1 - \delta M = 1 - \sum_{k,\ell} |(\nu_{\text{or}}(R_k, z_\ell) - \nu_S(R_k, z_\ell))|/2. \quad (1)$$

In this, δM is the mass fraction that is not located in the

same cell in both potentials, ν_{or} stand for the original density and ν_S stands for the density associated with the Stäckel potential. Double counting is avoided by dividing the sum by 2.

To calculate this, each orbit determined by a given set (E, J, I_3) , is integrated over a large number of periods, and its orbital density $\nu(R, z; E, J, I_3)$ (normalised to 1) is computed. This is done on a rectangular grid covering $[R_{min}(E, J), R_{max}(E, J)] \times [0, z_{max}(E, J)]$, by evaluating the time fraction spent in each cell.

In principle the orbit should be integrated until the orbital density reaches quasi-stationarity. This we may define by demanding that during a given time interval the value ν_{kl} in each cell (R_k, z_l) has varied by less than some small fraction. In practice, it takes an extremely long time to reach stationarity for orbits close to a resonance $m : n$ with m, n large, or having a moderate degree of stochasticity – these two cases being difficult to distinguish (*cf* Binney & Tremaine 1987, p.176).

Also modeling based on the Schwarzschild method has to deal with stationarity (see *e.g.* Schwarzschild 1993; Wozniak & Pfenniger 1997). Since modeling aims at constructing equilibrium models, only orbits for which the orbital density reaches stationarity in limited time (*i.e.* less than a Hubble time) need in principle to be taken into account. Accordingly, the non-stationary orbital densities would not need to be precisely reproduced in the Stäckel potential.

- *Conservation of I_3* : If locally a Stäckel potential is a good approximation, the Stäckel third integral I_3 should be approximately constant along the regular orbits. Since the goal is to provide a good approximation for an effective third integral for the largest possible number of orbits, the variation on I_3 should be made as small as possible. If possible, fits on smaller domains will be performed if this improves the approximation for the integral. The approximation is evaluated through the maximal variation of I_3 along the orbit with respect to its initial value, $\delta I_3 / I_3$.

On the other hand, one can argue that what really matters is a nominal variation of I_3 , $\delta I_3 / I_{3max}(E, J)$: for a given (E, J) , how precise can our identification of orbits be when we estimate the third integral of motion by I_3 within $[0, I_{3max}(E, J)]$? A related question is how precise this identification should be or, alternatively: how large is the tolerated variation on I_3 ?

The Stäckel potentials will be used as basis for a dynamical model. One of the aims of these models is to reveal the role of the third integral. Hence it is important to know that all structure caused by the dependence on this third integral can be traced. Consequently, the Stäckel potential should be precise enough, so that the uncertainty on the resulting approximation for I_3 is not larger than the scale of the smallest feature in I_3 of the distribution function. For example, in the limit where the dynamical model would turn out to be essentially 2-integral, there would be no need to set requirements on the constancy of I_3 .

This makes determining the maximum tolerance for errors in the fit to the potential an iterative process, which includes the modeling of the galaxy. First, a fit to the potential has to be obtained, and a model has to be constructed with that potential. The results of the model will then indicate whether the error on I_3 was small enough or not.

- *Topology of the orbits*:

As pointed out by Gerhard & Saha (1991), approximate conservation of I_3 along orbits alone does not ensure that I_3 provides a correct labelling for orbits (see also de Zeeuw & Merritt 1983). One still needs to check that the topology of orbital tori is similar to that of constant (E, J, I_3) surfaces: for then each orbit may be uniquely associated to one value of I_3 . This is done by comparing surfaces of section for orbits in the original potential, and $I_3 = cst$ curves for given (E, J) .

3 HOW TO OBTAIN A STÄCKEL POTENTIAL

The fitting procedure is derived from a deprojection method for triaxial systems presented in a paper by Mathieu & Dejonghe (1996). In that paper, a family of potential-density pairs is presented that can be used as building blocks for triaxial mass models. The spatial mass density and the potential can be both expressed in terms of the same basis functions.

Using this method, it would technically be possible to obtain a Stäckel approximation in two ways: (1) fitting the spatial mass density (2) fitting the potential.

The first way is not ideally suited for performing local fits since the calculation of a local value for the potential requires an integration of the density over the entire volume of the galaxy. In the case of a fit in a restricted part of space, there is obviously no control on the behaviour of the mass density at larger distances, and this can have serious implications for the potential obtained through integration. The correspondence between the forces generated by the original and the fitted potential, is likely to be a more useful indication for the quality of the approximation than the correspondence between the spatial densities. For a global fit on the other hand, it does make sense to construct a Stäckel potential through a fit on the spatial density.

The fitting procedure is based on a Quadratic Programming method. The aim is to find a linear combination of basis functions that provide a good approximation to the original function. When fitting the potential, the basis functions are

$$F(\tau) = -\frac{GM}{(d + \tau^p)^s}. \quad (2)$$

The basis functions and their coefficients are chosen by minimizing the variable

$$\chi^2 = \sum_{k, \ell} w_{k\ell} [f_{\text{original}}(r_k, z_\ell) - f_{\text{calculated}}(r_k, z_\ell)]^2, \quad (3)$$

with k and ℓ an index covering the grid points in the domain \mathcal{S}' . The weights $w_{k\ell}$ can be used to give different relative weights to the points in the grid, f stands for the function to fit.

In an ellipsoidal coordinate system $-\gamma \leq \nu \leq -\alpha \leq \lambda$, with α and γ negative, and the focal distance $\Delta = \sqrt{|\alpha - \gamma|}$ (de Zeeuw 1985), a Stäckel potential can be written as

$$V(\lambda, \nu) = g_\lambda F(\lambda) + g_\nu F(\nu), \quad (4)$$

with F an arbitrary function (here corresponding to (2)) and

$$g_\lambda = \frac{\lambda + \alpha}{\lambda - \nu}. \quad (5)$$

We now present the relevant formulas from Mathieu &

Dejonghe (1996), adapted for an axisymmetric system, that lead to an expression for the density in terms of the basic functions.

The expression for the axisymmetric density is

$$\rho(\lambda, \nu) = g_\lambda^2 \psi'(\lambda) + g_\nu^2 \psi'(\nu) + 2g_\lambda g_\nu \psi[\nu, \lambda], \quad (6)$$

where $\psi[\nu, \lambda]$ is the first order divided difference of ψ :

$$\psi[\nu, \lambda] = \frac{\psi(\lambda) - \psi(\nu)}{\lambda - \nu}, \quad (7)$$

and $\psi'(\lambda)$ is the derivative $\psi[\lambda, \lambda]$.

The connection between $\psi(\tau)$ and $F(\tau)$ (like in (2)) is given by

$$2\pi G\psi(\tau) = 2(\tau + \gamma)F'(\tau) - F(\tau) + 2\frac{\tau + \gamma}{\tau + \alpha}[F(\tau) - F(-\alpha)]. \quad (8)$$

The density can be expressed in terms of the basic functions by means of a third order divided difference:

$$\rho(\lambda, \nu) = H[\lambda, \nu, \lambda, \nu], \quad (9)$$

with $H(\tau)$ defined as:

$$H(\tau) = (\tau + \alpha)^2 \psi(\tau), \quad (10)$$

with $\psi(\tau)$ given in (8).

The divided difference of order $n-1$ of a function $G(\tau)$ is a function of the divided difference of order $n-2$, and is given by

$$G[\tau_1, \dots, \tau_n] = \frac{G[\tau_1, \tau_3, \dots, \tau_n] - G[\tau_2, \tau_3, \dots, \tau_n]}{\tau_1 - \tau_2}. \quad (11)$$

4 THREE TEST POTENTIALS

We build a smooth flattened model by combining a few spherical harmonics $Y_l^0(\theta)$ (Binney & Tremaine 1987), as follows:

$$\begin{aligned} \rho(r, \theta) &= C[\rho_0(r)Y_0^0(\theta, \phi) + \beta\rho_2(r)Y_2^0(\theta, \phi) \\ &+ \frac{|\beta|}{5}\rho_4(r)Y_4^0(\theta, \phi)], \end{aligned} \quad (12)$$

$$\rho_0(r) = \frac{1}{(1+r^2)^2} \quad (13)$$

$$\rho_2(r) = \frac{r^2}{(1+r^2)^3} \quad (14)$$

$$\rho_4(r) = \rho_2(r). \quad (15)$$

β is a parameter which determines the flattening ($\beta < 0$ for oblate systems). We set $C = 2/(\pi\sqrt{\pi})$ for a total mass equal to 1. This simple choice for the model ensures $\rho \propto r^{-4}$ and a fairly constant flattening. The resulting density for $\beta = -0.3$ is shown in figure 3. It is nearly ellipsoidal, with axis ratio $b/a \simeq 0.8$. We will in the following refer to the corresponding potential as Ψ_{ell} .

The corresponding potential is

$$\begin{aligned} \psi_{\text{ell}}(r, \theta) &= -4\pi GC[\psi_0(r)Y_0^0(\theta, \phi) + \beta\psi_2(r)Y_2^0(\theta, \phi) \\ &+ \frac{|\beta|}{5}\psi_4(r)Y_4^0(\theta, \phi)], \end{aligned} \quad (16)$$

where the ϕ_l are related to the ρ_l terms by equation (2-122) in Binney & Tremaine (1987).

As explained in paragraph § 2, we use a grid in integral

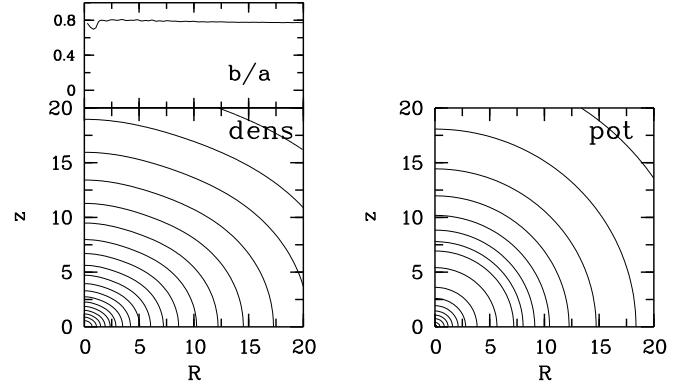


Figure 3. The spatial density, with its axis ratio, and potential corresponding to Ψ_{ell} , given by the sum of harmonics given in equation (12) and equation (16), with $\beta = -0.3$.

space that defines the domains for the fit. The grid contains 16 points in E (noted E_i), 7 points in J (noted J_i) and 7 angles ω_i .

For each of the domains, a fit can be produced, based on the χ^2 of equation (3), if the focal distance Δ is set. The choice of Δ of the spheroidal coordinate system affects the quality of the fit. An average Δ is obtained by computing a number of orbits in the original potential, and evaluating the focal distance for which sections of the $\lambda = cst$ ellipses most closely follow the inner and outer envelopes $R_{\text{min}}(z)$, $R_{\text{max}}(z)$ of the orbits. Of course, there is more variation in Δ for the more extended domains S' .

We started with a global fit for the potential Ψ_{ell} , i.e. a fit in the largest domain S' (extending to about 180 in R and in z), corresponding to the orbits that have $(E_{16}, 0)$. We take $J = 0$ instead of J_1 in order to avoid that orbits with smaller E should not be covered by the potential because their $J < (J_1)_{E_{16}}$.

This combination $(E_{16}, 0)$ is obviously the most unfavorable for the fit, and the variations in I_3 are expected to set a standard for the worst case: the maximum $(\delta I_3)_{\text{max}}$ for all 7 orbits with different ω_i is taken as the maximum tolerable variation. We demand that the variation of I_3 along the orbits with lesser spatial extent (i.e. $E' > E_{16}$, $J' > 0$ and the 7 ω_i , with (E', J') on the grid in integral space) is not worse than this. In this case, it turns out that the variation on I_3 is larger for orbits with (E_{15}, J_1) . Thus the next fit is done in the domain S' determined by $(E_{15}, 0)$.

After this fit, $(\delta I_3)_{\text{max}}$ is the error on I_3 for the orbits with (E_{15}, J_1) and this new value is now used to decide on the next fit. In this way, fits are done in the domains corresponding to $(E_{16}, 0)$, $(E_{15}, 0)$, $(E_{14}, 0)$, $(E_{11}, 0)$, $(E_2, 0)$ and $(E_1, 0)$.

If the correspondence between the orbits in a fitted and original potential happens to be very bad, it could be due to a poor correspondence between the force components of both potentials. Therefore, prior to the calculation of the orbits, it is useful to check the behaviour of the force components in the fitted and the original potential. Figure 4 shows the contours for the force components generated by Ψ_{ell} (full lines) with the Stäckel potential for the domain $S'(E_{11}, 0)$ (dashed lines) in overlay. Since the force components in both poten-

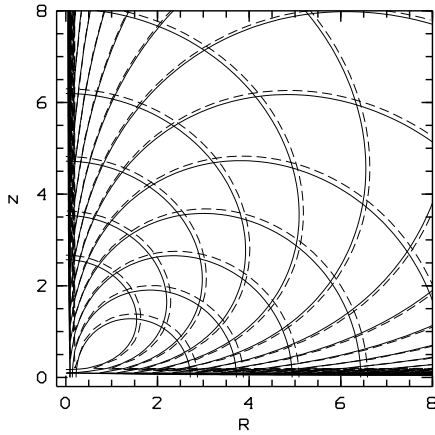


Figure 4. The contours for the two force components generated by Ψ_{ell} (full lines) and the Stäckel potential for the domain $S'(11,0)$ (dashed lines).

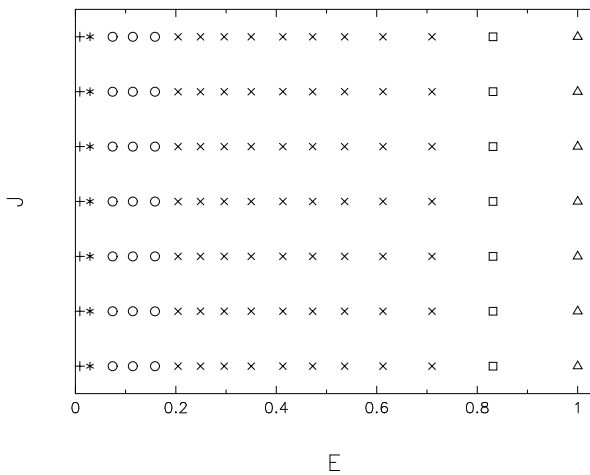


Figure 5. The (E, J) -grid for Ψ_{ell} , with different symbols for different potentials. We used a set of 6 Stäckel potentials to approximate the original potential.

tials do not appear too different, it is sensible to proceed with the comparison of integrated orbits.

In figure 5 the points in the (E, J) -grid for Ψ_{ell} are displayed as an example of how a set of potentials can be built; different symbols indicate the different potentials used. As can be seen from the different symbols, some potentials of the set are used for a small number of orbits, while others are used for a large number of orbits. The fact that the potential fitted in the largest domain is only used for orbits with only one value for E (indicated by the pluses) suggests that this method can really improve the approximation. Also the orbits that remain close to the centre seem to require a potential fitted in a limited part of space.

As a second trial case, a boxy density, with potential Ψ_{box} , is obtained from a combination of harmonics as described in (12) and (16) with $\beta = -0.5$, and has an axis ratio $b/a \simeq 0.6$. The contours are shown in figure 6. We also

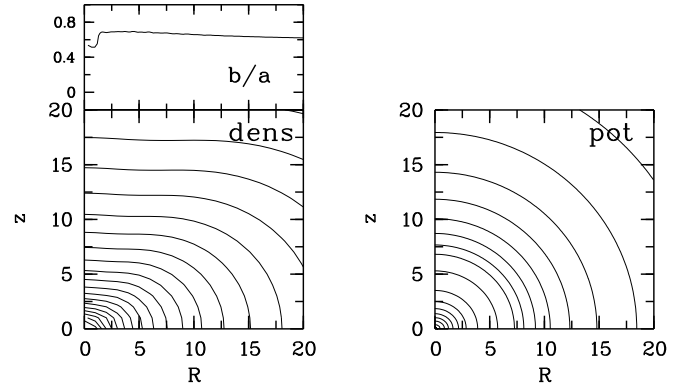


Figure 6. The spatial density, its axial ratio and the potential corresponding to Ψ_{Box} , given by the sum of harmonics given in equation (12) and equation (16), with $\beta = -0.5$.

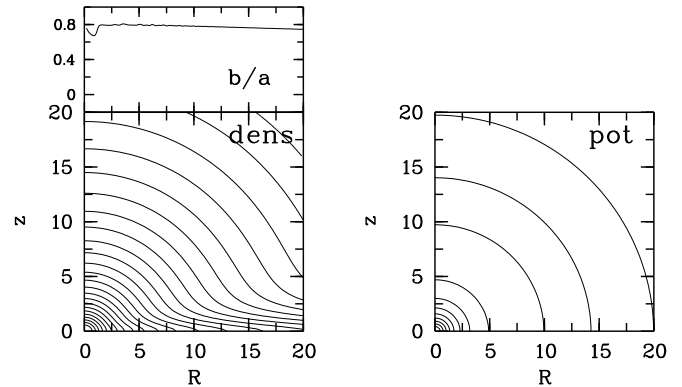


Figure 7. The spatial density, its axial ratio and the potential for a Miyamoto-Nagai potential with $b/a \sim 0.7$. The contours for the spatial density are strongly disk-like.

used a $16_E \times 7_J \times 7_{I_3}$ grid and approximated Ψ_{box} with a set of 8 Stäckel potentials.

Also a Miyamoto-Nagai (MN) potential with intermediate flattening, $b/a \sim 0.7$, is taken as trial potential. MN models exhibit very strong diskiness in the density contours, as can be seen in figure 7. This means that we are considering a difficult case, that is actually on the verge of being unrealistic for elliptical galaxies.

The grid has the same dimensions as the one described in the previous section. The MN potential is approximated with 8 potentials, the set of Stäckel potentials is constructed following the same strategy.

5 PRESENTATION OF THE RESULTS

5.1 Surfaces of section

Typical surfaces of section display (R, v_R) at $z = 0$, for the orbits having $v_z > 0$ when they cross the equatorial plane or display (z, v_z) for $v_R = 0$, for those orbits having $v_R > 0$ just after crossing.

The SoS's immediately tell us that for the three potentials, all orbits of our phase-space grid have an effective third integral. Stochasticity, if present, was mild and would have

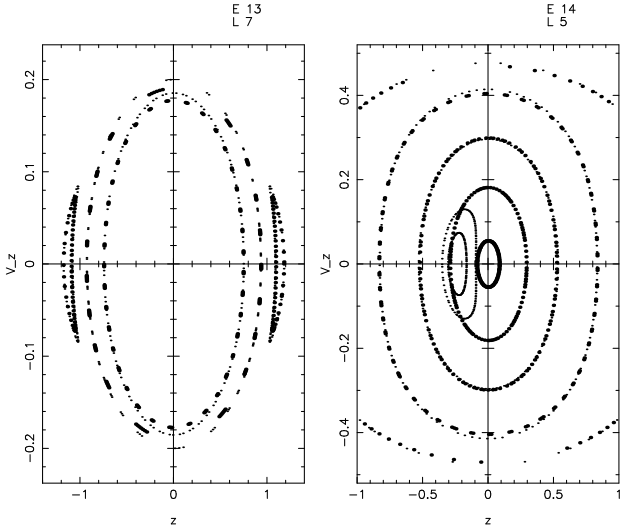


Figure 8. Surfaces of section for typical orbits in the MN potential (small dots) and the Stäckel potential (large dots).

required very long integrations to be visible on the SoS's. We did not carry out such integrations, because the SoS's were only meant as a preliminary check. In practice, anyway, mildly stochastic orbits behave very much like regular orbits, and we can hope to approximate them by an orbit in a Stäckel potential.

For ψ_{ell} and ψ_{box} , all orbits in our library have similar SoS's in both potentials. There is no evidence for stochasticity, nor for unrecovered minor families. For the MN potential, all orbits also appear as regular, but we found a few unrecovered minor orbital families.

Most of the orbits trapped around resonant tube orbits – what we called ‘minor orbital families’ in §2.3 – were present in the local Stäckel potential.

In figure 8 SoS's of a few orbits are displayed for the MN potential (small dots) and the Stäckel potential (large dots). Both panels show a ‘minor resonance’ evidenced by small ‘islands’. In the left panel, showing orbits with large I_3 , the orbits trapped around minor resonances are well reproduced within the Stäckel potential. The right panel displays orbits with smaller I_3 . Two orbits are trapped around a 1:1 resonance which does not exist in the Stäckel potential. They are examples of unrecovered minor orbital families. They are always found for small values of I_3 . Therefore, they correspond to orbits remaining close to the equatorial plane, where the MN potential is very much distorted by a strong diskiness.

Even for such extreme ‘diskiness’, these orbits only represent $< 1\%$ of the orbit library for MN. These obviously are orbits that we will not be able to take into account when building a model that uses Stäckel potentials. Although the unrecovered minor families are only a small fraction of the entire orbital library, we will exclude them from the statistics of the other checks discussed hereafter. As such, we are not taking those orbital families into account that no one expects to be approximated by a Stäckel potential.

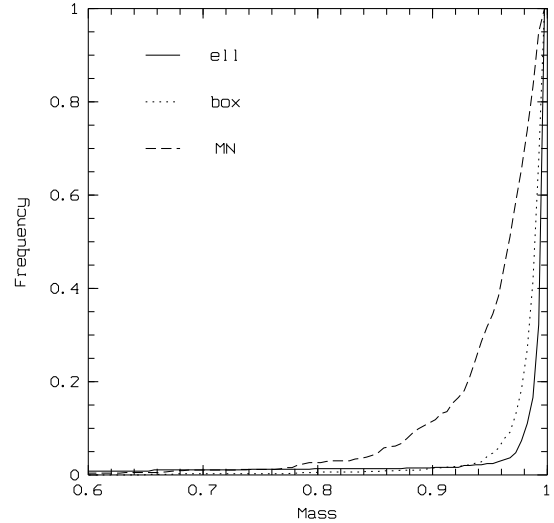


Figure 9. Cumulative distribution for the fraction of mass ‘correctly located’ in the orbital densities. The full line is for Ψ_{ell} , the dotted line is for Ψ_{box} and the dashed line for MN.

5.2 Orbital weights

For every orbit, the conserved mass fraction MC is calculated following equation (1), using a 20×20 grid in (R, z) . We integrate each orbit for at least $50 T_\Omega$, at most $200 T_\Omega$. We check every $50 T_\Omega$ whether quasi-stationarity has been reached. Quasi-stationarity is assumed when for every cell the orbital density has varied by less than 1% in $50 T_\Omega$.

The results are presented in figure 9 which gives the cumulative distribution for MC , the fraction of mass ‘correctly located’ in the orbital densities. A few orbital densities for MN have $MC < 60\%$, these correspond to minor resonances that were not fitted by our Stäckel potentials. Excluding those, the average MC is 99% for Ψ_{ell} , 98% for Ψ_{box} and 95% for MN.

5.3 How constant is the Stäckel I_3 ?

For every potential, the conservation of I_3 along the orbits is estimated by computing the relative variation $\delta^r \equiv \delta I_3(E, J, I_3)/I_3(E, J, I_3)$. At given (E, J) , the maximum of this quantity is derived among orbits with different I_3 : $\delta^r_{\text{max}} \equiv \max_{i=1,7}[\delta I_3(E, J, I_{3,i})/I_3(E, J, I_{3,i})]$.

Figure 10 shows how $\log(\delta^r_{\text{max}})$ is affected as more potentials are added to the set approximating ψ_{ell} .

The black dots represent the E ($J = 0$) of the domain \mathcal{S}' where the potentials are fitted. Dark gray shades represent small variations on I_3 , light gray shades represent larger variations. For each new local potential that is considered, a number of previously void cells of the (E, J) grid are filled and a number of values are replaced by new ones. It is clear that adding new potentials to the set improves the conservation of the third integral along the orbits, the difference between the global fit (upper left panel of figure 10) and the results of the complete set (lower right panel) is remarkable.

In the left panels of figure 11 we present histograms of δ^r for from top to bottom: ψ_{ell} , ψ_{box} and MN. For the MN potential, the resonances absent from the Stäckel ap-

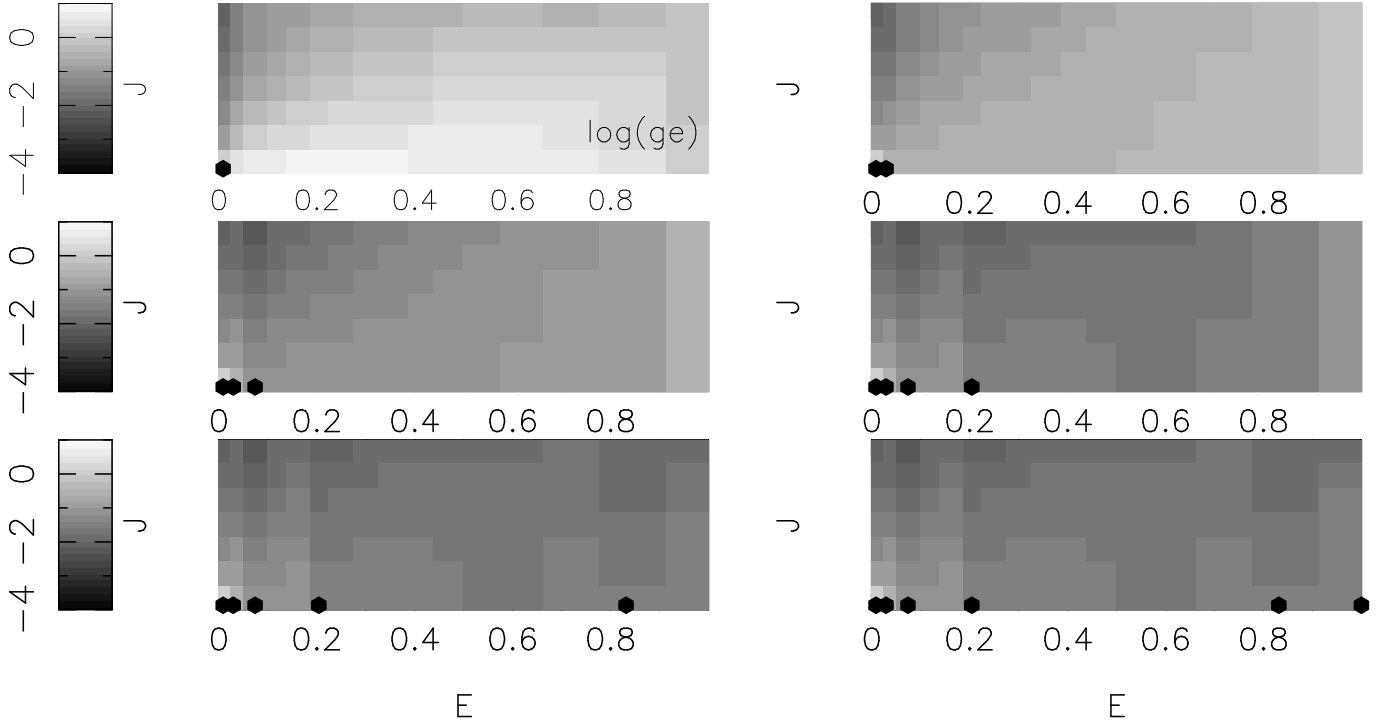


Figure 10. The evolution in $\log(\delta^r)$ as more potentials are added to the set of Stäckel potentials approximation Ψ_{ell} . The black dots indicate the E of the domain where the potentials were fitted ($J = 0$ for all six potentials). Dark (*resp.* light) gray shades represent small (*resp.* large) variations on I_3 .

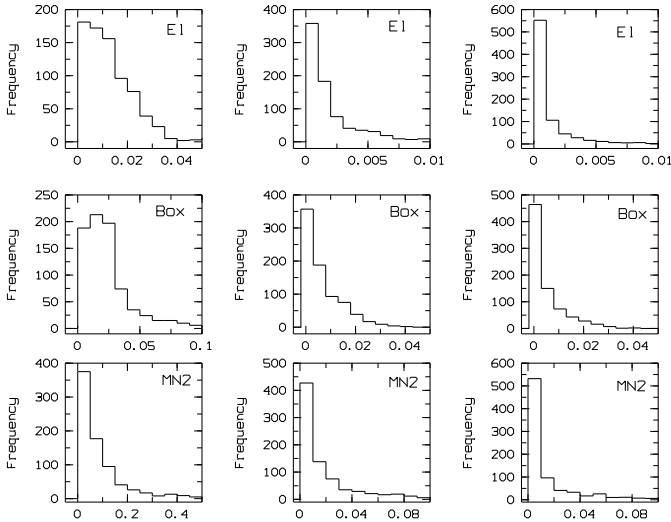


Figure 11. Histograms of δ^r in the left panels, δ^n (i.e. δI_3 normalised to $I_{3\text{max}}(E, J)$) in the middle panels and of δI_3 normalised to $I_{3\text{max}}(E)$ in the right panel.

proximation are not considered, a complete orbital library contains 784 orbits.

The average for δ^r is 2% for ψ_{ell} , while 75% of the orbits have $\delta^r < 1.7\%$. For ψ_{box} the average for δ^r is $\sim 2.6\%$ and 75% of the orbits have $\delta^r < 2.7\%$. For MN, the average value is $\sim 10\%$, and 75% of the orbits have $\delta^r < 12\%$. The

variation of δ^r along each orbit is of the order of the fitting error on the derivatives of the potential.

In the middle panels of figure 11 the results in terms of a nominal variation $\delta^n \equiv [\delta I_3(E, J, I_3)/I_{3\text{max}}(E, J)]$ are shown. For the nearly ellipsoidal potential Ψ_{ell} , 75% of the orbits have $\delta^n < .3\%$, with an average value of $\sim .2\%$. For Ψ_{box} the average is $\sim .7\%$ while 75% of the orbits have $\delta^n < 1\%$. For MN, the average value is $\sim 1.7\%$ and 75% of the orbits have a nominal error on I_3 less than 2.3%.

Dehnen & Gerhard (1993) used a similar indicator, but they normalised δI_3 to $I_{3\text{max}}(E)$, which gives smaller values for the nominal variation, as can be seen in the right panels of figure 11. The average for respectively Ψ_{ell} , Ψ_{box} and MN is .1%, .5% and 1.3%.

5.4 Topology of constant I_3 varieties

We plot on the same graph (figure 12): (i) the (R, \dot{R}) SoS of orbits as they cross the $z = 0$ plane (with $\dot{z} > 0$) in the original potential; and (ii) the invariant curves defined by $I_3 = cst$ (at $z = 0$). This is shown here for some intermediate value of E (E_4 of our grid) and $J = 0$. Radial orbits are in principle difficult to map, because of the transition between loop and box orbits (see Gerhard & Saha 1991). They are however very well described here, both for Ψ_{ell} and Ψ_{box} . The agreement is somewhat poorer in the case of MN for the transition region between box and loop orbits; however, the topology is still correctly described, in the sense that we can establish a one-to-one correspondence between the two sets of curves. This shows that I_3 may be used to label the orbits.

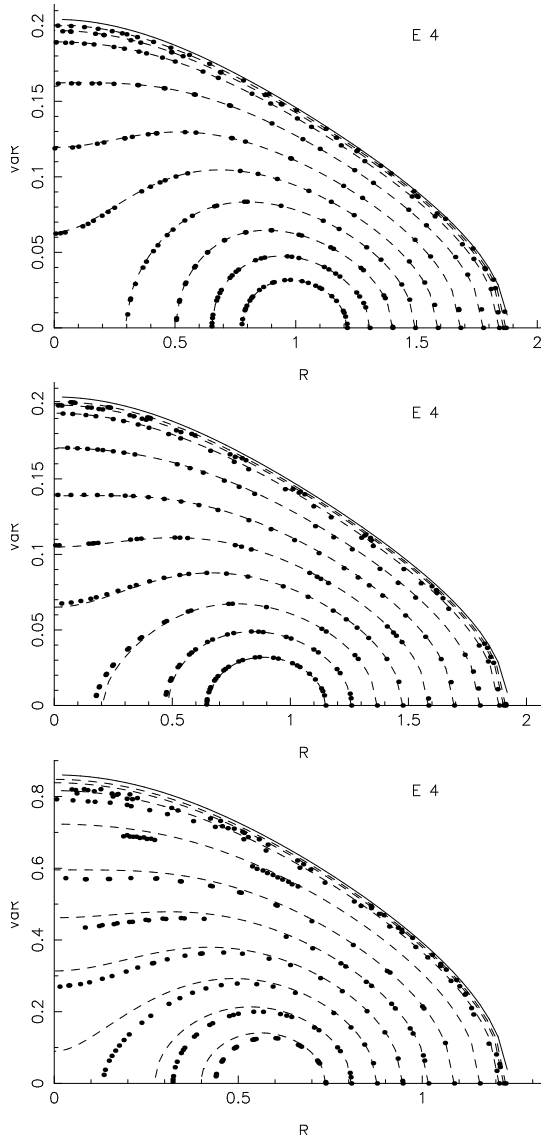


Figure 12. Comparison of SoS's and I_3 level curves at given $(E_4, J = 0)$, for Ψ_{ell} (upper panel), Ψ_{box} (middle panel), and MN (lower panel). Dots: surfaces of section (R, \dot{R}) at $z = 0$ with $\dot{z} > 0$. Lines: the intersection of $I_3 = cst$ surfaces with the $z = 0$ plane.

6 DISCUSSION

For the construction of dynamical models, the use of Stäckel potentials yields a number of advantages, amongst them (1) the property that the density and dynamical moments can be calculated analytically and (2) the absence of regularisation problems. Finally, once the dynamical model has been completed, the distribution function is known in an easy to use and analytical form. Though these models require a special form of the potential, they offer a great flexibility during the further modeling process. In a Stäckel potential there is a function of 1 variable that can be freely chosen. This freedom is advantageous, and can, of course, be exploited at the fullest when performing a fit to the galaxy potential.

Analogous to local Stäckel potentials, dynamical models built within this approximation will yield local distribution functions, simply because we have adapted the coordi-

nate systems in each domain \mathcal{S} where a local Stäckel potential is constructed. The use of a QP-method (Dejonghe, 1989) for dynamical modeling gives a large freedom for the basis functions. In this case, we can use basis functions for the distribution function that contribute only in limited parts of integral space. In practice, these limited parts will correspond to the rectangles \mathcal{R} from the local potentials.

The fact that the space of Stäckel potentials has measure zero in the space of all axisymmetric potentials, raises the obvious concern whether Stäckel potentials are suitable for the representation of any galaxy potential.

The scientific objections cluster around the following arguments:

(1) ‘What about central cusps?’ Indeed, central density cusps generally cannot be generated by a Stäckel potential in an ellipsoidal coordinate system. However, Sridhar & Touma (1997) showed that a Stäckel potential in parabolic coordinates can create a central cusp. Whether these potentials can be used in the scheme we propose here remains to be investigated. On the other hand, it may well be possible that there is no point in providing a good approximation to the third integral in regions where the cuspsiness of the density becomes important. Indeed, it is likely that the central density cusps are related to the presence of a central massive object (see *e.g.* review by Kormendy & Richstone 1995; Richstone et al. 1998). This may cause a higher fraction of ergodic orbits over a Hubble time. Such orbits will fill regions of phase-space where the distribution function depends essentially on the energy, or, for less ergodic regions, also on angular momentum (*cf* Merritt 1999). The fraction of regular to ergodic motion in a real galaxy stands as a major unknown. The most popular scenario at the moment is that ergodicity has gradually been introduced in the system, as orbits that pass close to the central mass concentration were perturbed by it (Gerhard & Binney 1985; Valluri & Merritt 1998). One may then suppose that the original orbital tori which have not been disrupted still underlie most of the features in phase-space— with essentially homogeneous 6-D density between them.

(2) ‘Does a Stäckel approximation allow an accurate fit to a typical galactic potential?’ As was already noticed for some time, the main orbit families found by numerical integration in general triaxial potentials are present in a Stäckel potential (Schwarzschild 1979; de Zeeuw 1985), but obviously there is no place in an integrable potential for smaller orbital families nor stochastic orbits. These minor orbital families appear to occupy only a small volume fraction of phase-space, as long as figure rotation is unimportant (Gerhard, 1985; Binney, 1987). In practice, Stäckel potentials do turn out to provide reasonably good global fits for systems without central mass concentration (Dejonghe et al. 1996) or for regions beyond the influence of the central mass concentration (Emsellem et al. 1999). It is true that the use of one single Stäckel potential assumes a single confocal system where the streamlines of the mean stellar motion coincide with the coordinate lines of the ellipsoidal coordinate system. Hence, the construction of such a single Stäckel potential inevitably involves some sort of averaging (de Zeeuw & Lynden-Bell 1985; Dejonghe & de Zeeuw 1988), and is not always considered to be a sufficiently general approach (at least in triaxial cases, Binney 1987; Merritt & Fridman 1996). However, the use of confocal streamlines seems to be

a valid assumption for individual orbits (Anderson & Statler 1998). Moreover, studying logarithmic potentials, those authors find that the mean velocities can be well fitted using local coordinate systems with confocal coordinate lines, with the focal distances taken within a fairly narrow range. Our approach allows to carry this idea one step further, on the level of the distribution function.

7 CONCLUSIONS

In this paper, we present an extension of the available approximations for the effective third integral in axisymmetric systems, obtained by using a set of Stäckel potentials as representation for a galaxy potential, instead of one single Stäckel potential. We have studied the feasibility and effectiveness of this method.

The creation of a set of local Stäckel potentials is done through a fit on the system potential. There is a large freedom in the choice of the domains where the local fits are done and the composition of the set of Stäckel potentials. The set of approximating local potentials can be extended until the desired precision is obtained.

We have tested the method on three potentials: (A) a harmonical potential (Ψ_{ell}) that behaves very smoothly with a nearly ellipsoidal density; (B) a harmonical potential (Ψ_{box}) with a boxy density; and (C) a Miyamoto-Nagai model (MN) with a density that has an exaggerated disk structure.

As one may expect, the model with smallest diskiness/boxiness is easiest to approximate using sets of Stäckel potentials. But what really motivates this study is to check the estimate made for the effective third integral, if we approximate it by the third integral I_3 that the Stäckel potentials define.

The quality of the approximation is checked in several ways: (1) surfaces of section, that reveal possible resonances and irregular orbits, (2) conservation of orbital weights, which is important for the reconstruction of the spatial density, (3) conservation of I_3 along the orbits, in order to validate the labeling of orbits, (4) topology of the orbital space. The conservation of orbital weights and the conservation of I_3 are the criteria that can be best expressed numerically.

According to the expectations, the approximation of Ψ_{ell} has orbits that are very similar to the orbits in the original potential, as can be judged from the surfaces of section and the topology. The results for the conservation of orbital weights (an average of 99% for Ψ_{ell}) and I_3 ($\delta^r \equiv \delta I_3(E, J, I_3)/I_3(E, J, I_3) \sim 2\%$ and $\delta^n \equiv [\delta I_3(E, J, I_3)/I_{3\text{max}}(E, J)] \sim .2\%$ for Ψ_{ell}) confirm the quality of the approximation.

The method also proves to be successful for Ψ_{box} , with an average of 98% for the conservation of orbital weights, $\delta^r \sim 2.6\%$ and $\delta^n \sim .7\%$. The SoS's and the topology of the orbits also confirms this good result.

The success of the method on the Miyamoto-Nagai potential is somewhat less, because of the strong diskiness. Still, using a small set of Stäckel potentials, we are able to reproduce most orbits with satisfactory accuracy, except for a few resonances. The resonances that are not reproduced by the set of Stäckel potentials, all have small values of I_3 , i.e. the orbits lie in the region where the diskiness is im-

portant. Leaving this resonances out of consideration, the orbital weights seem to be well conserved (on average 95% for MN) and the topology of the orbits is well reproduced. Also for these potentials, the Stäckel I_3 can be used as label for the orbits ($\delta^r \sim 10\%$ and $\delta^n \sim 1.7\%$). The potentials of observed elliptical galaxies are generally rounder than the strongly disk Miyamoto-Nagai models.

Given the positive results found for the three rather different models considered, it seems to be possible, using a reasonable number of local Stäckel potentials, to provide good approximations for a third integral, suitable for labeling orbits in dynamical models.

With respect to existing approximations for a third integral in axisymmetric systems, the advantage of this new one is mainly that, while it can be envisaged for application to systems with arbitrary flattening, it also yields a simple analytic expression for the approximate third integral locally. This method will be fully exploited if it is used to build, for roughly axisymmetric galaxies, explicit distribution functions that depend on three integrals.

REFERENCES

- Anderson R.F., Statler T.S., 1998, ApJ, 496, 706
 Batsleer P., Dejonghe H., 1994, A&A, 287, 43
 Binney J.J., 1987, in Structure and Dynamics of Elliptical Galaxies, T. de Zeeuw, ed., (Dordrecht: Reidel), p229
 Binney J.J., Spergel D., 1982, ApJ, 252, 308
 Binney J.J., Tremaine S., 1987, Galactic Dynamics, Princeton University Press, Princeton
 Binney J.J., Davies R.L., Illingworth G.D., 1990, ApJ, 361, 78
 Carpintero D.D., Aguilar L.A., 1998, MNRAS, 298, 1
 Dehnen W., Gerhard O.E., 1993, MNRAS, 261, 311
 Dejonghe H., 1989, ApJ, 343, 113
 Dejonghe H., de Zeeuw P.T., 1988, ApJ, 329, 720
 Dejonghe H., De Bruyne V., Vauterin P., Zeilinger, W.W., 1996, A&A, 306, 363
 de Zeeuw P.T., 1985, MNRAS 216, 273
 de Zeeuw P.T., Lynden-Bell D., 1985, MNRAS, 215, 713
 de Zeeuw P.T., Merritt D., 1983, ApJ, 267, 571
 de Zeeuw P.T., Evans N.W., Schwarzschild M., 1996, MNRAS, 280, 903
 Emsellem E., Dejonghe H., Bacon R., 1999, MNRAS, 303, 495
 Evans N.W., Häfner R.M., de Zeeuw P.T., 1997, MNRAS, 286, 315
 Gerhard O., 1985, A&A, 151, 279
 Gerhard O., Binney J., 1985, MNRAS, 216, 467
 Gerhard O.E., Saha P., 1991, MNRAS, 251, 449
 Kent S.M., de Zeeuw P.T., 1991, AJ, 102, 1994
 Kormendy, J., Richstone, D. 1995, ARA&A **33**, 581-624.
 Mathieu A., Dejonghe H., 1996, A&A, 314, 25
 Matthias M., Gerhard O., MNRAS, submitted, astro-ph/9901036
 Merritt D., 1999, PASP, 111, 129
 Merritt D., Fridman T., 1996, ApJ, 460, 136
 Papaphilippou Y., Laskar J., 1996, A&A, 307, 427
 Papaphilippou Y., Laskar J., 1998, A&A, 329, 451
 Petrou M., 1983, MNRAS, 202, 1195
 Richstone D.O., 1982, ApJ, 252, 496
 Richstone D.O., Ajhar E.A., Bender R., Bower G., Dressler A., Faber S.M., Filippenko A.V., Gebhardt K., Green R., Ho L.C., Kormendy J., Lauer T.R., Magorrian J., Tremaine S., 1998, Nature 395, 14
 Rix H.-W., de Zeeuw P.T., Cretton N., van der Marel R.P., Carollo C.M., 1997, ApJ, 488, 702

- Schwarszchild M., 1979, ApJ 232, 236
Schwarszchild M., 1993, ApJ, 409, 563
Sridhar S., Touma J., 1997, MNRAS 292, 657
Valluri M., Merritt D., 1998, ApJ, 506, 686
van de Hulst H.C., 1962, Bull. Astr. Inst. Neth., 16, 235
Verhulst F, 1979, RSLPT, 290, 435
van der Marel R.P., Cretton N., de Zeeuw T.P., Rix H.-W., 1998,
ApJ, 493, 613
Wozniak H., Pfenniger, D., 1997, A&A, 317, 14